Quasilinear ridge structures in water surface waves

R. Blümel,* I. H. Davidson,† and W. P. Reinhardt‡
Department of Chemistry, University of Pennsylvania, Philadelphia, Pennsylvania 19104-6323

H. Lin and M. Sharnoff
Department of Physics, University of Delaware, Newark, Delaware 19716
(Received 17 June 1991; revised manuscript received 16 September 1991)

Nodal patterns of stationary capillary waves formed on the surface of water enclosed in an agitated ripple tank with circular and stadium-shaped cylindrical walls are examined in the low-frequency ($\nu < 50$ Hz) and high-frequency ($\nu > 700$ Hz) regimes. In the low-frequency regime, in agreement with predictions of quantum-chaos theory, the shape of the tank's boundaries (integrable or nonintegrable) dictates the type of nodal patterns obtained. In the high-frequency regime we obtain nodal patterns characterized by short-range order (called "scarlets" because they are believed to be the precursors of quantum scars), as recently predicted in the quantum-chaos context by P. O'Connor, J. Gehlen, and E. J. Heller [Phys. Rev. Lett. **58**, 1296 (1987)].

PACS number(s): 03.40.Gc, 05.45.+b, 03.65.Ge, 03.40.Kf

Contrary to physical intuition, a superposition of monochromatic plane waves with random amplitudes, phases and propagation directions does not result in a distribution of amplitudes that resembles a laser speckle pattern (see Fig. 1 for a numerical simulation of a speckle pattern) but exhibits a network of quasilinear ridge structures (see Fig. 2). This surprising result was recently obtained by O'Connor, Gehlen, and Heller [1]. The ridge structures predicted in Ref. [1] were subsequently called "scarlets" [2] since they are believed to be the precursors of quantum scars [2]. The scarlet conjecture was based on convincing arguments and detailed numerical calculations. Although presented in the context of quantum chaos, it is possible (and the authors of Ref. [1] allude to it) that scarlets are a general wave phenomenon. This point of view is supported by the experiments of Burke at the University of California at Santa Cruz, who obtained ridge structures very similar to scarlets in an optical experiment using laser light [2]. We will demonstrate below that scarlets can also be observed as a network of capillary waves forming on a water surface. Thus, Burke's laser experiments and our experiments with water surface waves provide strong evidence for the ubiquity of scarlets in many fields of physics.

We use the following experimental setup. A Plexiglas container with cylindrical walls and a flat transparent Plexiglas bottom is filled with water, approximately 5 mm deep. The container is placed on an overhead projector which maps any disturbances of the water surface into a black-and-white pattern on a projection screen. This way the patterns can easily be demonstrated to an audience or

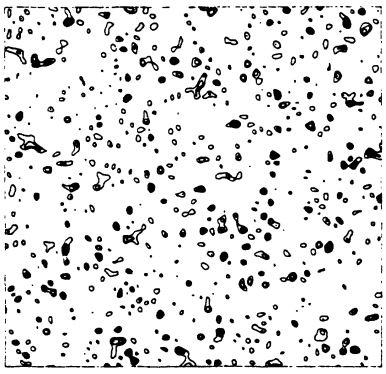

FIG. 1. Speckle pattern obtained by superposition of 1000 cosine waves with various wave-vector magnitudes (from Fig. 1(c), Ref. [1]).

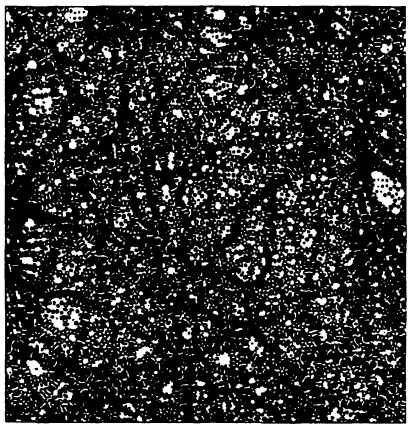

FIG. 2. Contour plot of the resulting total amplitude of a superposition of 400 cosine waves, each with a random propagation direction, phase, and amplitude, but the *same* wavelength (from Fig. 1(a), Ref. [1]).

recorded with a camera. Water surface waves are generated by driving the container at a fixed frequency with an electromechanical shaker. We used a Gearing & Watson shaker type GWV 4/2 driven sinusoidally by a HP 8111A oscillator via a Radio Shack MPA90 amplifier. Due to the constant depth of the water layer and the single-frequency drive, the wavelength λ of the resulting water surface waves is constant over the total area of the tank. A constant wavelength is important because a superposition of waves with random wavelengths in addition to random phase and direction is predicted [1] to result not in scarlets (Fig. 2) but in a speckle pattern (Fig. 1). We used two tank shapes for our experiments. A round tank (radius $R=53$ mm; see Fig. 3) and a stadium-shaped tank consisting of two semicircular end pieces (radius $R=53$ mm) and two straight sections (length $L=41$ mm; see Fig. 4).

The wave velocity $\mathbf{u}$ of the irrotational, propagating part of the water surface waves generated in the tank can be derived from a velocity potential ϕ,

$$\mathbf{u}=\nabla\phi \ . \tag{1}$$

For small surface disturbances, the case considered exclusively in the following, a linear theory applies and ϕ satisfies the Laplacian equation

$$\Delta_{\perp}\phi=0 \ . \tag{2}$$

This equation has to be solved together with the boundary condition

$$\frac{\partial^2\phi}{\partial t^2}+G(k)\frac{\partial\phi}{\partial z}=0 \ , \tag{3}$$

which holds at $z=0$. The function G in (3), which depends on the wave number $k=2\pi/\lambda$, is given by

$$G(k)=g+\rho^{-1}Tk^2 \ . \tag{4}$$

Here, $g=9.81$ m/s^2 is the gravitational constant, $\rho=10^3$ kg/m^3 is the density of water, and $T=0.074$ N/m is the water surface tension. For surface waves with $\lambda>1.7$ cm, the first term in (4) predominates and $G=g$ is a good approximation. These waves are appropriately called "gravity waves" [3]. In our experiments, however, λ will be much smaller than 1.7 cm and the second term in (4) is dominant. Waves of this type are called "capillary waves" [3].

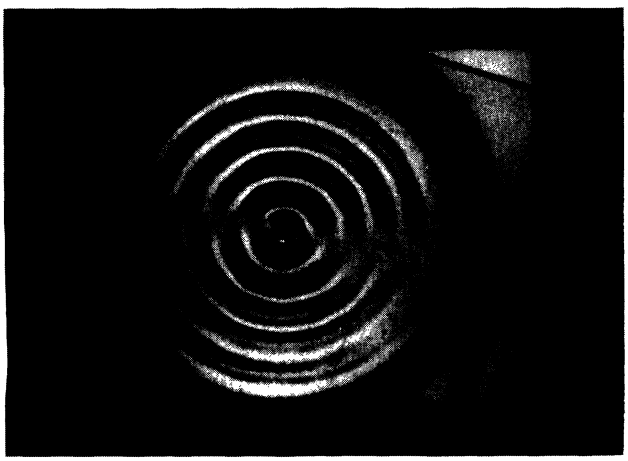

FIG. 3. Bessel-function pattern in the round ripple tank.

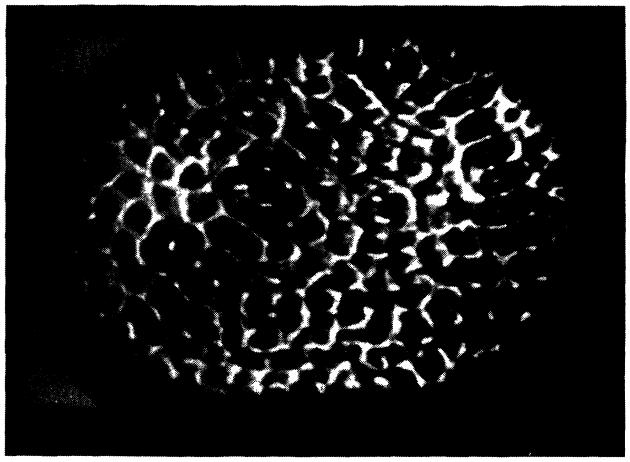

FIG. 4. Complicated stationary wave pattern in the stadium-shaped ripple tank which corresponds to a nonseparable boundary condition. The pattern resembles wave-function nodal patterns obtained by solving numerically Schrödinger's equation with a stadium-shaped cylindrical potential. A scar is also visible in this figure.

The z coordinate ζ of the disturbed water surface (the undisturbed flat surface being characterized by $\zeta\equiv0$), can be derived from the velocity potential via [3]

$$\zeta=-\frac{1}{G(k)}\frac{\partial\phi}{\partial t} \ . \tag{5}$$

The Laplacian equation (2) is easily solved with the separation ansatz [3]

$$\phi=e^{kz}e^{i\omega t}f(x,y) \ . \tag{6}$$

The boundary condition (3) is fulfilled for

$$\omega=\sqrt{G(k)k} \tag{7}$$

and the Laplacian equation (2) is solved if

$$\frac{\partial^2 f}{\partial x^2}+\frac{\partial^2 f}{\partial y^2}+k^2 f=0 \ . \tag{8}$$

Since $\zeta=(-1/G)\partial\phi/\partial t=(-i\omega/G)\phi$, the nodal structure of f is identical with the nodal structure of the surface elevation ζ, which we observe directly with our projection technique. We note that the simplest type of solutions of (8) are plane waves, which is the basis of our analog demonstration of the scarlets predicted in Ref. [1].

The Helmholtz equation (8) recalls the two-dimensional stationary Schrödinger equation which would apply (with Dirchlet boundary condition) to a quantum particle enclosed within the boundaries of the (empty) water tank and restricted to move in the x-y plane. The difference in boundary conditions notwith-

standing, the two-dimensional stationary Schrödinger equation and the Helmholtz equation (8) possess similar types of solutions, especially with respect to the issue of separability (round container) and nonseparability (stadium-shaped container), which nowadays is a central issue in the study of quantum systems with a chaotic classical limit. For the round enclosure, e.g., the Helmholtz equation (8) trivially separates in cylindrical coordinates (r,θ). Its solutions are Bessel functions $f_{mn}(r,\theta)=J_m(k_{mn}r)e^{in\theta}$, $m=0,1,2,\ldots$, $n=1,2,3,\ldots$, where $k_{mn}=x_{mn}/R$ with $J'_m(x_{mn})=0$ and R is the radius of the tank. For $m=0$, e.g., these solutions can readily be demonstrated in the round wave tank (see Fig. 3). Additional patterns ($m>0$), characterized by great symmetry and esthetic beauty, can be obtained at other discrete driving frequencies [4]. The stadium-shaped wave tank, on the other hand, corresponds to a nonseparable situation and, judging from the corresponding quantum-mechanical problem [2,5–7], complicated wave patterns are expected for the solutions of (8) with the boundary condition (3). Indeed, only for very low driving frequency ($\nu<10$ Hz), do we find simple wave patterns, some of which can be interpreted as "bouncing ball" patterns [2,4]. At higher driving frequencies, but in the same frequency range as was used to generate Fig. 3, we find complicated wave patterns like the pattern shown in Fig. 4. This pattern resembles in its degree of complexity the nodal patterns obtained by solving the quantum Schrödinger equation for a particle moving in a two-dimensional stadium-shaped enclosure [2,5,7]. A scar [2] is also visible in this figure. It is seen as a quasiorderly arrangement of wave fronts along a triangular classical bouncing orbit.

Summarizing the first part of our experiments, we can say that the differences between an integrable and a nonintegrable boundary condition, an issue currently much discussed in the theory of nonintegrable quantum systems, can convincingly be demonstrated with water surface waves.

We now turn to the main point of our paper, the demonstration of scarlets in water surface waves. For this purpose, we have to work in the "semiclassical" regime, i.e., at a very high driving frequency $\nu=\omega/2\pi$ which corresponds to a very small wavelength λ relative to the dimensions of the enclosure. Driving the stadium-shaped tank at $\nu=777$ Hz ($\lambda=1$ mm), we obtained the nodal pattern shown in Fig. 5. The similarity of this pattern with the numerically generated scarlet pattern (Fig. 2) is striking. Figure 5 clearly shows the network of ridge structures predicted in Ref. [1]. Stationary patterns very similar to the patterns displayed in Fig. 5 appeared at other driving frequencies, e.g., at 817,945,1210,... Hz.

We note that the detailed appearance of the (stationary) scarlet patterns depends sensitively on the shape of the tank, the shaking frequency and amplitude, and the water depth. The scarlet phenomenon itself, however, is completely robust against these factors and will always appear as a network with short-range order very similar to the network shown in Fig. 5.

Although demonstrating convincingly several nontrivial points predicted by wave chaos theory, a more quantitative discussion of our experiments is now in order. Similar to the experiments by Gollub and collaborators [8,9] we digitized Fig. 5 by scanning it electronically with a 200-mm-focal-length charge-coupled-device camera (Photometrics, Int. Model No. CH 230) at a distance of approximately 3 m. The image was then transferred to a Macintosh IIX computer via a CE 200 electronics unit coupled to a CC 200 controller interface. The dynamical range of the digitized picture was approximately 10^4 with 400×400 pixels resolution. The corresponding set of numerical data z_{mn}, $m=1,\ldots,400$, $n=1,\ldots,400$ was then spooled to an IBM3090 mainframe computer where its discrete Fourier transform $\hat{z}_{K,K'}$, $K=1,\ldots,400$, $K'=1,\ldots,400$ was calculated. The absolute squares $|\hat{z}_{K,K'}|^2$, $K=1,\ldots,70$, $K'=1,\ldots,70$ of the resulting 400×400 Fourier amplitudes are presented in Fig. 6 as an intensity plot of the Fourier plane. Clearly visible is a ring at $\kappa=(K^2+K'^2)^{1/2}\approx53$, which corresponds to the monochromatic excitation frequency at 777 Hz. The width of the ring extracted from a plot of the radial in-

FIG. 5. Scarlets in the stadium-shaped ripple tank at $\nu=777$ Hz.

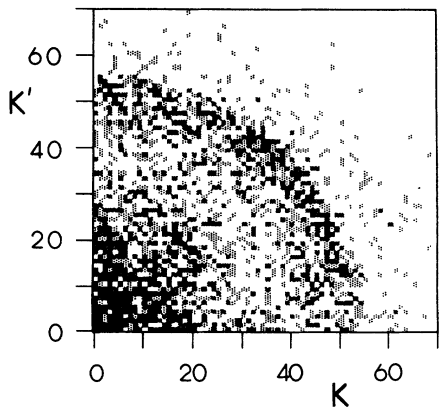

FIG. 6. Intensity plot of the discrete Fourier transform $\hat{z}_{KK'}$ of Fig. 5. The darker a pixel, the larger the magnitude of $|\hat{z}_{KK'}|^2$.

tensity distribution corresponds to $\Delta\nu \approx 50$ Hz. The ring shows an approximately uniform angular distribution, which is consistent with a uniformly random distribution of plane-wave directions. The Fourier amplitudes in the ring are exponentially distributed consistent with the hypothesis of a Poissonian random process. The correlation coefficient

$$\rho = \frac{\langle A\varphi \rangle - \langle A \rangle \langle \varphi \rangle}{\sigma_A \sigma_\varphi} \tag{9}$$

of the Fourier amplitudes A and angles φ, where the averages are taken over the ring region $40 \leq \kappa \leq 60$, was also calculated. We obtained $\rho = -0.024$. The standard deviation of ρ is $\Delta\rho = 1/\sqrt{N-3}$ for N data points. For $N = 1643$ data points this amounts to $\Delta\rho = 0.025$. This result is statistically consistent with $\rho = 0$, i.e., no correlation between amplitudes and angles. The region around $K, K' \approx 0$ was not explored in detail. However, a plot of the radial intensity of the Fourier plane reveals that the peak at $\kappa \approx 53$ rises from a smooth background which the region around $K, K' \approx 0$ is part of. It is possible, and expected, that the background (and especially the intensity in the small-K region) represents the effects of viscous damping, image distortions due to the overhead projector optics, film response, and discretization noise. The peak at $K = K' = 0$, e.g., is trivial and corresponds to the average brightness of Fig. 5.

In summary, at low driving frequencies we see the difference in the appearance of wave patterns of water surface waves depending on the specific type (integrable or nonintegrable) of boundary conditions as predicted by quantum-chaos theory [2,4,–7]. At high driving frequencies (the semiclassical limit) we observe the scarlet patterns predicted in the quantum-chaos context in Ref. [1]. We gave evidence that the wave pattern shown in Fig. 5 is indeed the result of a random superposition of plane waves which makes the appearance of short-range order all the more surprising. Thus we have demonstrated that the appearance of scarlets is a phenomenon that applies to the physics of water surface waves in the same way as it does to random matter waves in quantum chaos. Besides these two wave domains, we expect to see scarlets in random superpositions of monochromatic elastic waves, electromagnetic waves (laser, radar, microwaves), and acoustic waves. Thus, scarlets are a universal phenomenon of interdisciplinary importance.

It is a pleasure to acknowledge financial support by the NSF under Grant Nos. CHE-8819436 and DCB-8821065. R.B. is grateful for financial support by the Deutsche Forschungsgemeinschaft. Many thanks are due M. Heald and L. Westling at Swarthmore College for providing experimental equipment in the initial stages of our experiments. I. H. D. acknowledges the Regional Laser and Biotechnology Laboratories where this work was carried out.

*Present address: Department of Physics, University of Delaware, Newark, DE 19716.
†Present address: Department of Psychology, University of Pennsylvania, Philadelphia, PA 19104.
‡Present address: Department of Chemistry, BG-10, University of Washington, Seattle, WA 98195.

[1] P. O'Connor, J. Gehlen, and E. J. Heller, Phys. Rev. Lett. **58**, 1296 (1987).
[2] E. J. Heller, in *Chaos and Quantum Physics,* 1989 Les Houches Lecture Notes, edited by A. Voros, M. Gianonni, and O. Bohigas (North-Holland, Amsterdam, 1990).
[3] J. Lighthill, *Waves in Fluids* (Cambridge University Press, Cambridge, England, 1978).
[4] R. Blümel, Habilitationsschrift, Technical University, Munich, 1990 (unpublished).
[5] S. W. McDonald and A. N. Kaufman, Phys. Rev. Lett. **42**, 1189 (1979).
[6] O. Bohigas, M. J. Giannoni, and C. Schmit, Phys. Rev. Lett. **52**, 1 (1984).
[7] H.-J. Stöckmann and J. Stein, Phys. Rev. Lett. **64**, 2215 (1990).
[8] S. Ciliberto and J. P. Gollub, J. Fluid Mech. **158**, 381 (1985).
[9] F. Simonelli and J. P. Gollub, J. Fluid Mech. **199**, 471 (1989).

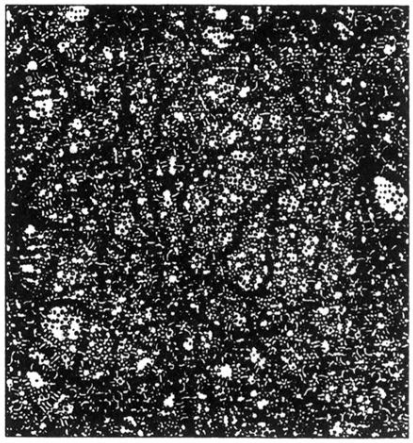

FIG. 2. Contour plot of the resulting total amplitude of a superposition of 400 cosine waves, each with a random propagation direction, phase, and amplitude, but the *same* wavelength (from Fig. 1(a), Ref. [1]).

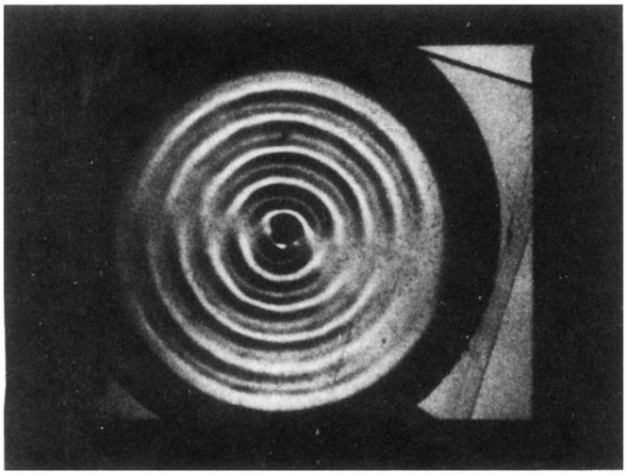

FIG. 3. Bessel-function pattern in the round ripple tank.

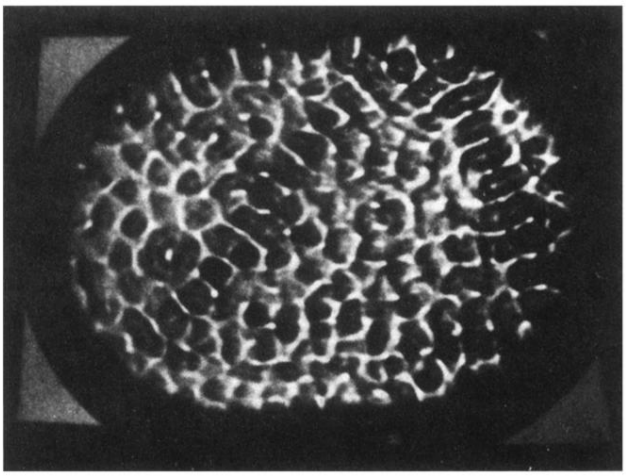

FIG. 4. Complicated stationary wave pattern in the stadium-shaped ripple tank which corresponds to a nonseparable boundary condition. The pattern resembles wave-function nodal patterns obtained by solving numerically Schrödinger's equation with a stadium-shaped cylindrical potential. A scar is also visible in this figure.

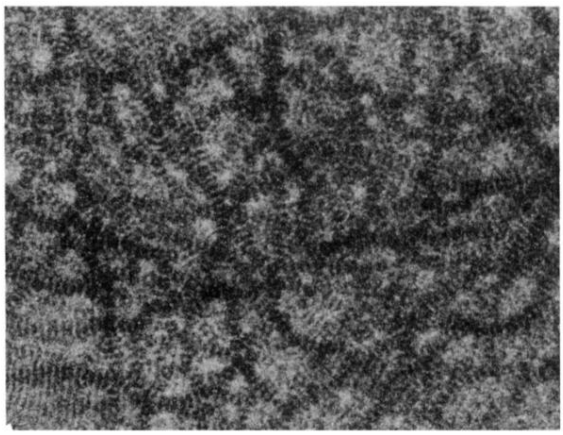

FIG. 5. Scarlets in the stadium-shaped ripple tank at $\nu = 777$ Hz.

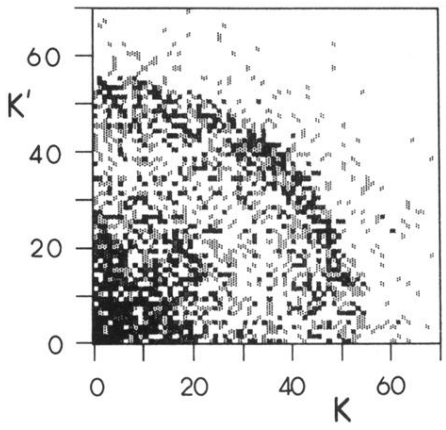

FIG. 6. Intensity plot of the discrete Fourier transform $\hat{z}_{KK'}$ of Fig. 5. The darker a pixel, the larger the magnitude of $|\hat{z}_{KK'}|^2$.